Supporting Information

Nuclear Quantum Effects in Hydrophobic Nanoconfinement

Buddha Ratna Shrestha[1*], Sreekiran Pillai[1*], Adriano Santana[1], Stephen H. Donaldson Jr[2], Tod A. Pascal[3†], Himanshu Mishra[1†]

[1]King Abdullah University of Science and Technology (KAUST), Water Desalination and Reuse Center (WDRC), Biological and Environmental Sciences and Engineering (BESE) Division, Thuwal 23955 - 6900 Saudi Arabia
[2]Département de Physique, Ecole Normale Supérieure / PSL Research University, CNRS, 24 rue Lhomond, 75005 Paris, France
[3]ATLaS Laboratory, Department of NanoEngineering and Chemical Engineering, University of California San Diego, La Jolla, CA 92023 USA

[*]These authors contributed equally to this work

buddha.shrestha@kaust.edu.sa, sreekiran.pillai@kaust.edu.sa, adriano.santanasanchez@kaust.edu.sa, steve.donaldson@phys.ens.fr, himanshu.mishra@kaust.edu.sa, tpascal@ucsd.edu

[†]Corresponding authors: himanshu.mishra@kaust.edu.sa, tpascal@ucsd.edu

I. Sample preparation:

In this work, we quantified the hydrophobic forces between extended surfaces in H_2O and D_2O. The extended surfaces were back-silvered mica rendered hydrophobic with covalently bonded perfluorodecyltrichlorosilane (FDTS). The process of sample preparation and characterization of the hydrophobic layer is described below.

I.1. Back-silvered mica preparation for FDTS deposition

We used Norland Optical Adhesive 61(NOA 61) for gluing silver-backed mica to the SFA glass disks. The silver was deposited on mica (thickness of ~ 50 nm) using an electron beam evaporator at a pressure equal to or below 2.66×10^{-6} mbar at a rate of 0.5 Å/sec to ensure the highest possible quality. A tiny drop of the glue was applied to the SFA disk and was allowed to spread uniformly to form a thin film. Silvered mica of thickness ≈ 5 μm thick was placed on top, with the silver side facing the glue. These disks were cured by ultraviolet light with maximum absorption in the range of 320-380 nm for one hour. Once cured, the glue can withstand temperatures up to 533 K. This heat resistance is the main advantage of using NOA 61 as our SFA sample preparation requires vacuum baking at 393 K.

I.2. Hydrophobic functionalization of mica films

Covalently grafted hydrophobic layers of thiols and silanes can be achieved easily on gold and silica surfaces, respectively. For our experiments, we needed to achieve similar hydrophobic layers on mica film surfaces. Unfortunately, mica is chemically inert due to the low number density of hydroxyl groups available to participate in silanation reactions[1-3]. In order to activate mica, we used an oxygen-plasma activation process incorporated with steam. Pressure inside the chamber was first brought down to 0.2 mbar and later maintained at 0.8 mbar when oxygen was introduced. Under these conditions, the samples were exposed to plasma (50 W) for one hour. The plasma activated mica surfaces were rendered hydrophobic by vapor phase deposition of perfluorodecyltrichlorosilane (FDTS) using a molecular vapor deposition (MVD) setup, Applied Microstructures MVD100E (Figure S1). Prior to deposition of FDTS, the leak rate inside the chamber and deposition lines were maintained below 2.66×10^{-3} mbar/min by constant nitrogen purging. Molecular vapor deposition of FDTS involved two cycles of deposition, each cycle having four FDTS injections at a pressure of 6.6×10^{-3} mbar and one injection of water vapor at 8×10^{-3} mbar. A reaction time of 15 minutes was allowed between cycles to aid the bonding of FDTS molecules to the activated mica surfaces. The samples were then annealed at 393 K at a pressure of 30.3 mbar for an hour to graft a covalently bonded solid layer of FDTS (Figure S1). We then rinsed the FDTS-deposited samples thoroughly with tetrahydrofuran (THF), followed by annealing at 30.3 mbar and 363 K for 60 minutes to remove the physisorbed FDTS layers on mica, as shown in Figure S2a and b.

We produced thiolated surfaces on mica-templated gold that was glued onto silica disks. These samples were immersed in 1 mM solutions of the desired thiol in ethanol for

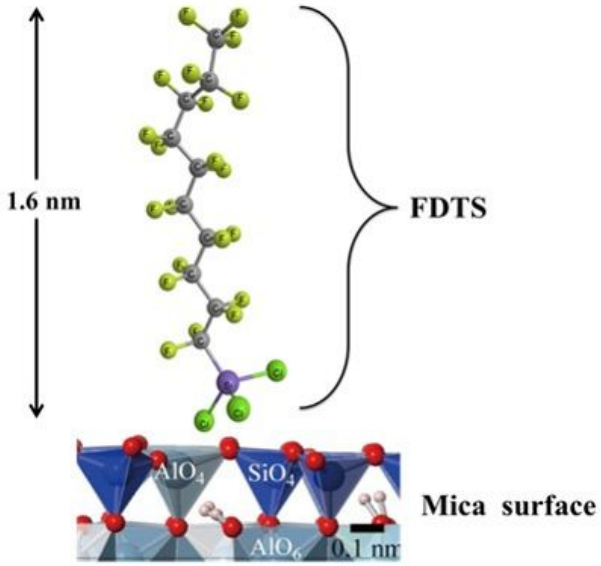

12-18 hours, shielded from light. Subsequently, the surfaces were washed with hexane and ethanol and dried with dry N_2 gas[4].

Figure S1: Ball-and-stick representation of the perfluorodecyltrichlorosilane (FDTS) and mica

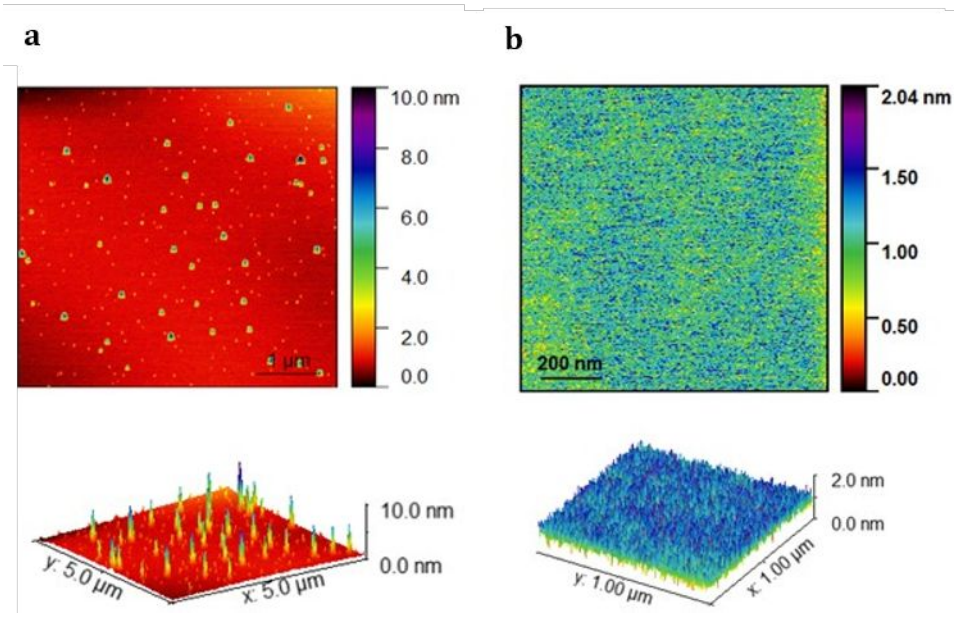

Figure S2: **a)** Atomic force micrographs of the vacuum-baked FDTS/mica surface (rough); **(b)** FDTS/mica surface after rinsing with tetrahydrofuran followed by additional vacuum baking.

I.3. TEM characterization of hydrophobic layer on mica:

For TEM characterization, we applied a layer of gold (50 nm) over the FDTS layer. The difference in contrast to the 3 different layers in the TEM image (Figure S3) proves the presence of the FDTS layer sandwiched between the mica and gold layers.

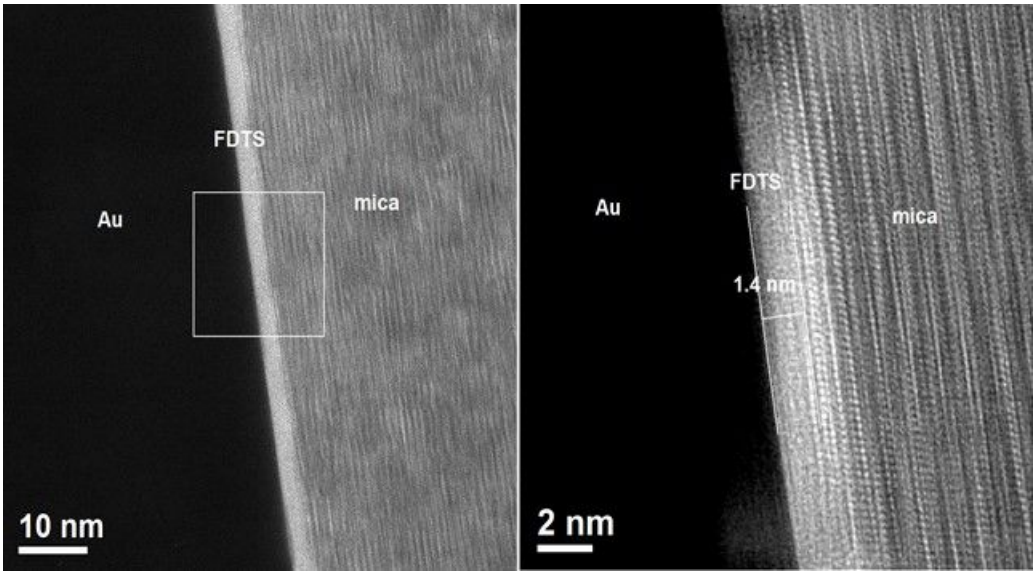

Figure S3: TEM image of FDTS sandwiched between the mica and gold layers

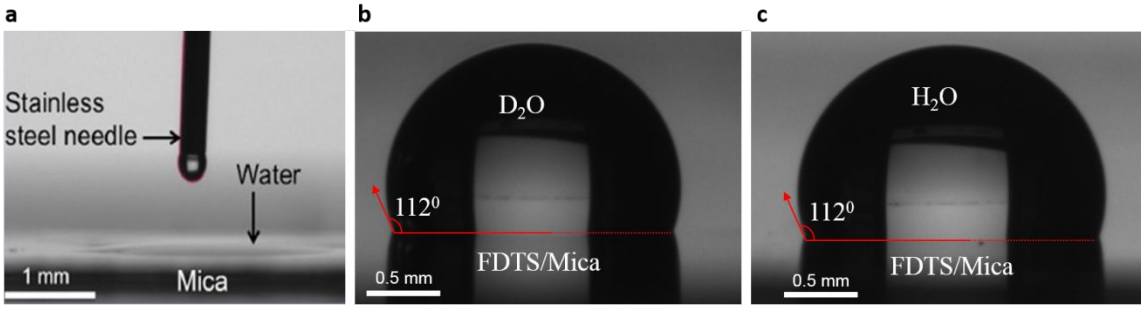

Figure S4: **a)** Wetting of mica with water: H_2O and D_2O water spread on mica yielding ultralow contact angles; **b-c)** Sessile drops of H_2O and D_2O placed gently on FDTS/mica surfaces yield contact angles that are indistinguishable.

I.4. Properties of light and heavy water:

Table S1a compares properties of liquid H_2O and D_2O at 298 K and 1 atm (unless stated otherwise[5,6])

Property	**H_2O**	**D_2O**	**Difference**
Hydrogen bond length (Å)	1.74	1.81	3.03%
Number of hydrogen bonds	3.62 ± 0.1	3.76 ± 0.1	3.86%
Tetrahedrality	0.576	0.593	2.95%
Refractive index (η)	1.32844	1.33335	0.37%
Dipole moment (D, 1D =3.34×10^{-30} Cm) (gas phase)	1.855	1.855	0
Liquid/vapor surface tension (mN/m)	71.98	71.87	-0.15%
Viscosity (mPaS)	0.8904	1.0966	23.2%
Molar density (mol/L)	55.35	55.14	-0.38%
Bond energies (kJ/mol) (gas phase)	458.9	466.4	1.6%
Melting point, T_m (K) (at 1 atm)	273.15	276.97	1.4%
Temperature of maximum density (K)	277.13	284.34	2.6%
Critical temperature (K)	647.1	643.85	-0.5%
Specific heat capacity, C_v [J/(Kmol)]	74.54	84.42	13.2%
Translational diffusion constant, Dx (Å^2/ps)	0.230	0.177	-23%
Rotational diffusion constant, D_θ (rad^2/ps)	0.104	0.086	-17%
Dielectric constant at 25 °C	78.39	78.06	0.42%
Dielectric relaxation time at 20 °C (ps)	9.55	12.3	29%
Water dimer dissociation energy (kJ/mol) (gas phase) 10 K	13.22	14.88	12.7%
Vibrational frequency (/cm) (gas phase)	3657.1 1594.7 3755.9	2671.6 1178.4 2787.7	

Table S1b demonstrates the stability of our FDTS-coated mica surfaces. We incubated samples in water for controlled durations of time, representative of the duration of our experiments. We then measured contact angles by advancing sessile drops of water (H_2O) of volume 6µl dispensed through a stainless-steel capillary and advanced/retracted at 0.2 µL-s^{-1}.

Incubation Time (h)	Intrinsic contact angle, θ_o	Advancing contact angle, θ_A	Receding contact angle, θ_R
0	$112° \pm 1°$	$118° \pm 2°$	$100° \pm 2°$
1	$111° \pm 2°$	$118° \pm 2°$	$100° \pm 2°$
2	$111° \pm 1°$	$118° \pm 2°$	$100° \pm 2°$
3	$110° \pm 1°$	$118° \pm 2°$	$100° \pm 2°$
4	$110° \pm 1°$	$117° \pm 2°$	$100° \pm 2°$
5	$110° \pm 1°$	$117° \pm 2°$	$100° \pm 2°$
6	$110° \pm 1°$	$117° \pm 2°$	$100° \pm 2°$

I.5. Measurement of hydrophobic forces between FDTS-coated mica surfaces:
We placed two FDTS deposited cylindrical disks with radius of curvature $R \sim 1 - 2$ cm in a crossed cylindered geometry in an SFA. We measured the interaction forces between the disks by bringing them into contact at ultralow speeds ~10 nm/s immersed in solutions of degassed 5 mM KCl (99.8% Fisher Scientific) and H_2O or D_2O. The solutions were degassed by reducing the pressure in the flask containing the solution. We stirred the solution continuously during the process. In order to prevent evaporation of water, we connected a Liebig condenser placed in an ice bath between the solution and the pump. The representative measured force-distance curves are shown in Figure S5. We measured the hydrophobic force (F) acting between the surfaces at a fixed distance, D, by force-distance spectroscopy from $F = k \times D_{jump}$, where D_{jump} is the distance between surfaces and k is the spring constant of the spring used in the system.

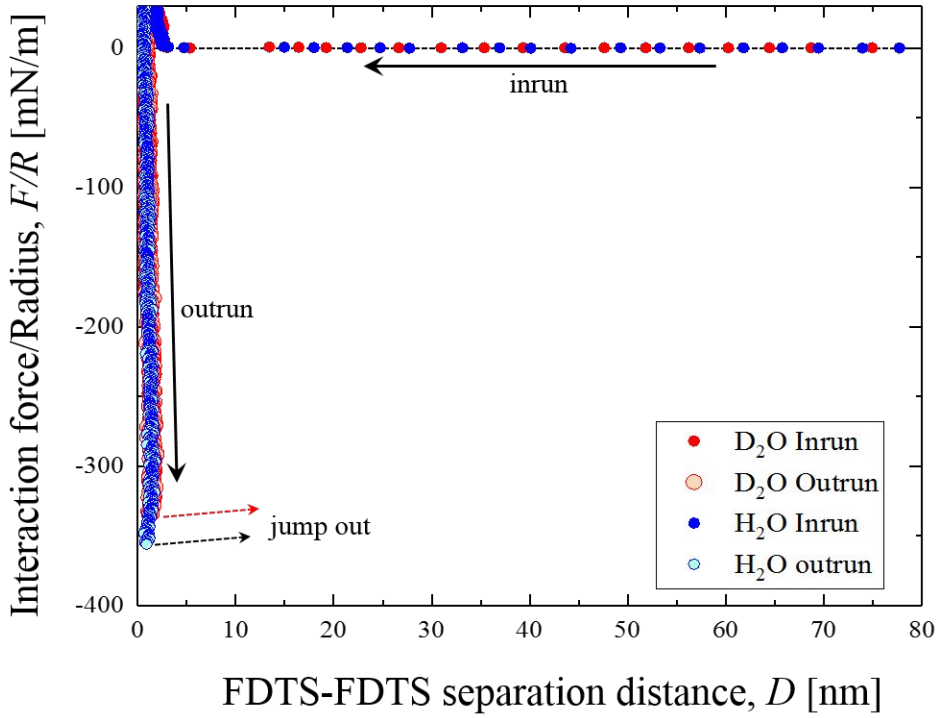

Figure S5: The interactive forces measured between mica coated with FDTS surfaces in 5 mM KCl solution of H_2O and D_2O. The representative force curves are shown. The outrun points for D_2O are enlarged for visibility.

We find that the surfaces attract each other due to the hydrophobic force, which is significant and measurable when the surfaces are $D \sim 10$ nm apart. The force increases with decreasing distance between the surfaces. The total force acting between the opposing FDTS/Mica surfaces at the closest distance is determined by separating the surfaces at a constant speed. We found that hydrophobic forces were ~10% higher in H_2O than in D_2O.

I.6 Calculation of Van der Waals force between FDTS coated surfaces in H_2O and D_2O:

We calculated the Hamaker constants for FDTS-H_2O-FDTS and FDTS-D_2O-FDTS systems by using the following equation[7]:

$$A_H = \frac{3kT}{4}\left(\frac{\varepsilon_1 - \varepsilon_3}{\varepsilon_1 + \varepsilon_3}\right)\left(\frac{\varepsilon_2 - \varepsilon_3}{\varepsilon_2 + \varepsilon_3}\right) + \frac{3h\nu_e}{8\sqrt{2}}\left[\frac{\left(\eta_1^2 - \eta_3^2\right)\left(\eta_2^2 - \eta_3^2\right)}{\left\{\left(\eta_1^2 + \eta_3^2\right)\left(\eta_2^2 + \eta_3^2\right)\right\}^{1/2}\left\{\left(\eta_1^2 + \eta_3^2\right)^{1/2} + \left(\eta_2^2 + \eta_3^2\right)^{1/2}\right\}}\right]$$

where ε_i (i = 1,2,3) are the dielectric constants for FDTS (we assumed it to be same as that of perfluoroethylene), H_2O and D_2O, respectively, as 2.1, 80, and 79.7; ηi (i =1, 2,3) refer to the refractive indices of perfluoroethylene, H_2O and D_2O, respectively, which are1.359, 1.3333, 1.328; $\nu_e = 3.0 \times 10^{15}\ s^{-1}$ is the main electronic absorption frequency in the ultra-violet region. Using the equation for the van der Waals force $F_{vdW} = -A_H/6D^2$, we estimate the maximum vdW force at the contact (D = 0.17 nm) for the FDTS-H_2O-FDTS and FDTS-D_2O-FDTS systems to be 17.9 mN/m and 18.4 mN/m at respectively.

II. Computational Section:

(A) Molecular Dynamics details

We initially minimized the forces in each system using the conjugate gradient minimization scheme with an energy tolerance of 10^{-4} and a force tolerance of 10^{-5}. We then slowly heated the system from 0 K to 298 K over 100 ps in the constant volume, constant temperature NVT (canonical) ensemble, using a Nose-Hoover thermostat (temperature relaxation constant of 100 fs). The equations of motion were integrated with the velocity verlet algorithm in a 1 fs timestep. We truncated the van der Waals forces at an outer and inner cutoff of 1.2 and 1.1 nm respectively, between which we employed a cubic spline so as to guarantee zero energy and forces at the outer cutoff. We truncated the short-range electrostatic interactions at 1.2 nm and evaluated the long-range electrostatics using the 2D-PPPM method[8] with a k-space tolerance of 10^{-6} kcal/mol. After initial equilibration, we annealed the system by cycling the temperature 5 times between 298 K and 550 K over 30 ps, followed by a further 100 ps of NVT dynamics at 298 K and then 1 ns of constant pressure, constant temperature (NPT) simulations using the Andersen barostat (pressure relaxation constant of 1 ps).
The equations of motion used are those of Shinoda et al.[9], which combine the hydrostatic equations of Martyna et al.[10] with the strain energy proposed by Parrinello and Rahman[11]. The time integration schemes closely follow the time-reversible measure-preserving Verlet integrators derived by Tuckerman et al.[12].

During the last 500 ps of the 1 ns NPT simulation, we calculated the average x and y cell lengths and adjusted the final NPT simulation cell linearly to the averages over a further 100 ps of dynamics. Finally, we performed 30 cycles of NVT dynamics, where the temperature was cycled from 298 K to 550 K over 250 ps, followed by 250 ps of NVT simulation at 298 K. We saved snapshots of the system (atomic position and velocities) every 10 ps and a restart file after each cycle. We then used a starting point for an additional 25 ps of NVT dynamics while saving the atomic positions and velocities every 2 fs.

(B) 2PT method details

In the 2PT method, we approximated the quantum corrections to the enthalpy from our classical MD trajectories by applying quantum corrected weighting functions to the vibrational density of states function[13] [DoS(ν)] at room temperature. These quantum corrections vanish at zero frequency (purely diffusive modes) and increase with increasing frequency[13] and are therefore more important for high energy vibrations.
For each sheet separation, we calculated the excess thermodynamic values by referencing a separate bulk water simulation. We note that this approach, while approximate, captures the critical zero-point energy and librational (heat-capacity) corrections which are in good aggrement[14] with more complete, though computationally expensive, path-integral simulations[15]. We also note that as previously demonstrated,[16] the quasi-harmonic approximation may overestimate the nuclear quantum effect. Other quantum corrections involving proton tunneling due to Fermi-Dirac and Bose-Einstein statistics are not included

here, however these effects are expected to be negligible at room temperature[13]. Note that as expected, quantum corrections significantly influence the thermodynamics of the bulk liquid (Table S2), including decreasing the isochore molar heat capacity by 37 J/mol/K for H_2O and 32.3 J/mol/K for D_2O. In both cases, quantum corrections improve the agreement with experimental results, as previously reported[17].

In each 2PT calculation, we took the effective volume of the nanoconfined water molecules to be an enclosed volume with $z = D - 3.75$Å, which accounts for the carbon–water van der Waals exclusion zone. We obtained the mean and standard deviation in our calculated thermodynamics and DoS functions from statistical averaging over the 2PT results of all 30 snapshots for each system. We also performed reference simulations of the bulk liquids (Table S2) and the thermodynamics evaluated using the 2PT method.

Table S2: Thermodynamic properties of H_2O and D_2O from equilibrium MD simulations using the TIP4P2005f water model. The calculated standard molar entropy S (J/mol/K), enthalpy H (kJ/mol), free energy G (kJ/mol), constant volume heat capacity C_v (J/mol/K) and zero-point energy ZPE (kJ/mol) are presented and compared to available experimental data. We define the enthalpy $H^0 = H_{vap} + 4RT - 6.9$ kJ/mol, where H_{vap} is the enthalpy of vaporization obtain from our simulations as $H_{vap} = U_{bulk} - U_{vac}$, 4RT is the ideal gas correction term, and the 6.9 kJ/mol is the dipolar correction term. Where appropriate, both the classical (C) and quantum (Q) energies are reported.

	$S^{(Q)}$	$H^{(C)}$	$H^{(Q)}$	$G^{(Q)}$	$C_v^{(C)}$	$C_v^{(Q)}$	ZPE
	J/mol/K	kJ/mol	kJ/mol	kJ/mol	J/mol/K	J/mol/K	kJ/mol
H_2O	60.6 ± 0.3	-36.5 ± 0.1	-25.7 ± 0.1	-43.8 ± 0.1	102.8 ± 7.4	65.8 ± 7.6	62.7 ± 0.1
-- Expt	69.9[a]		-36.1	-55.9		74.5[a]	55.4[b]
D_2O	66.7 ± 0.4	-36.8 ± 0.1	-26.4 ± 0.1	-46.3 ± 0.1	104.6 ± 8.8	72.3 ± 8.7	46.1 ± 0.1
-- Expt	75.64[c]		-35.5	-58.6		83.7[c]	40.5[b]

a: ref[18], b: ref[19] and c: ref[20].

Table S3: Thermodynamic properties of nanoconfined H_2O and D_2O from equilibrium MD simulations with the TIP4P2005f water model. The number of confined water molecules (N), the graphene sheet – sheet distance (*D* - Å), classic enthalpy (H^c – kJ/mol/molecule), quantum enthalpy (H^q – kJ/mol/molecule), entropy (S^q – J/mol/K/molecule), constant pressure heat capacity (C_v^q – J/mol/K/molecule) and zero-point energy (ZPE – kJ/mol/K/molecule) are provided for H_2O (top) and D_2O (bottom)

H_2O

N	*D*	H^c	H^q	S^q	C_v^q	ZPE
	Å	kJ/mol/molecule	kJ/mol/molecule	J/mol/K/molecule	J/mol/K/molecule	kJ/mol/K/molecule
162	6.6 ± 0.9	-30.0 ± 0.5	-18.9 ± 1.0	67.7 ± 1.9	6.1 ± 13.2	62.1 ± 1.4
286	9.4 ± 1.0	-34.9 ± 0.4	-23.2 ± 0.9	61.4 ± 1.9	14.5 ± 10.9	63.6 ± 1.2
438	12.4 ± 1.1	-34.7 ± 0.3	-23.1 ± 0.6	62.4 ± 1.4	22.2 ± 8.0	63.3 ± 0.9
566	14.9 ± 1.2	-35.1 ± 0.3	-23.4 ± 0.5	62.2 ± 0.9	25.8 ± 8.1	63.5 ± 0.8
722	18.0 ±1.2	-35.5 ± 0.2	-23.7 ± 0.4	61.2 ± 0.5	28.6 ± 6.1	63.6 ± 0.6
878	21.0 ± 1.1	-35.6 ± 0.2	-24.1 ± 0.4	61.3 ± 0.7	37.5 ± 9.7	63.4 ± 0.6
1172	26.9 ± 1.4	-35.9 ± 0.1	-24.4 ± 0.4	61.0 ± 0.5	44.0 ± 9.8	63.4 ± 0.5
1440	32.1 ± 1.3	-36.0 ± 0.1	-24.7 ± 0.3	61.0 ± 0.4	48.4 ± 8.8	63.2 ± 0.4
2194	46.6 ± 1.2	-36.2 ± 0.1	-25.0 ± 0.2	60.8 ± 0.2	53.3 ± 8.5	63.2 ± 0.3
2936	61.3 ± 1.3	-36.3 ± 0.1	-25.1 ± 0.2	60.7 ± 0.2	57.9 ± 9.7	63.1 ± 0.2

D_2O

N	*D*	H^c	H^q	S^q	C_v^q	ZPE
	Å	kJ/mol/molecule	kJ/mol/molecule	J/mol/molecule	kJ/mol/molecule	kJ/mol/molecule
162	6.6 ± 0.9	-30.3 ± 0.4	-20.2 ± 0.7	74.7 ± 1.6	9.8 ± 9.6	44.7 ± 0.9
286	9.4 ± 1.0	-35.3 ± 0.4	-24.7 ± 0.5	67.7 ± 1.7	17.2 ± 9.1	46.1 ± 0.8
438	12.3 ± 1.1	-35.0 ±0.2	-24.4 ± 0.4	68.3 ± 0.9	22.4 ± 7.5	46.1 ± 0.6
566	14.9 ± 1.2	-35.4 ± 0.2	-24.8 ± 0.3	68.1 ± 0.9	31.3 ± 6.1 9	46.1 ± 0.5
722	18.0 ± 1.1	-35.8 ± 0.2	-25.2 ± 0.3	67.3 ± 0.8	35.4 ± 8.4	46.2 ± 0.5
878	21.0 ±1.1	-36.0 ± 0.2	-25.4 ± 0.2	67.0 ± 0.6	41.8 ± 8.4	46.2 ± 0.4
1172	26.7 ± 1.1	-36.2 ± 0.2	-25.6 ± 0.2	66.9 ± 0.5	46.6 ± 9.3	46.2 ± 0.4
1440	31.8 ± 1.3	-36.3 ± 0.1	-25.9 ± 0.1	66.8 +/-± 0.5	50.0 ± 8.6	46.1 ± 0.3
2194	46.7 ± 1.2	-36.5 ± 0.1	-26.1 ± 0.1	66.6 ± 0.3	57.5 ± 9.5	46.1 ± 0.2
2936	61.0 ±1.1	-36.6 ± 0.1	-26.2 ± 0.1	66.6 ± 0.3	61.2 ± 10.5	46.1 ± 0.2

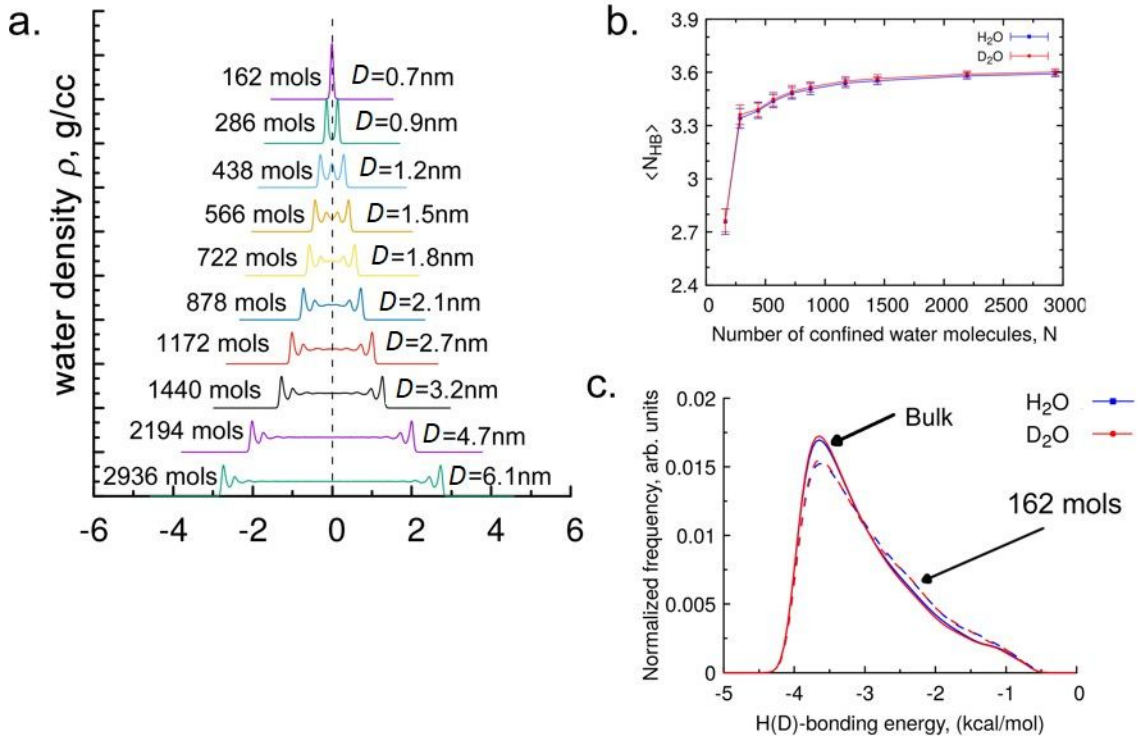

Figure S7: **Density and hydrogen bonding analysis. a.** Mass density profile of water on parallel graphene sheets from equilibrium MD simulations and the TIP4P2005f [21] forcefield. The number of water molecules and corresponding sheet separations are listed. Results for both H_2O and D_2O are shown **b.** An average number of hydrogen bonds per molecule for H_2O (blue) and D_2O (red) as a function of the number of confined molecules. The MD data (solid circles and squares) are connected with lines to guide the eyes. The error bars represent the standard deviation. **c.** Distribution of hydrogen (deuterium) bond energy for single layer H_2O (dashed blue line) and D_2O (dashed red line) compared to the bulk liquids (solid lines). The energy function is based on the Dreiding[22] definition: $E_{HB} = \epsilon\left[5\left(\frac{\sigma}{r_{ij}}\right)^{12} - 6\left(\frac{\sigma}{r_{ij}}\right)^{10}\right]\cos^4(\theta_{ijk})$, where ε = 4.75 kcal/mol, σ = 2.75Å, is the O – O donor acceptor distance and θ_{ijk} is the O-H(D) … O donor-hydrogen(deuterium)-O acceptor angle

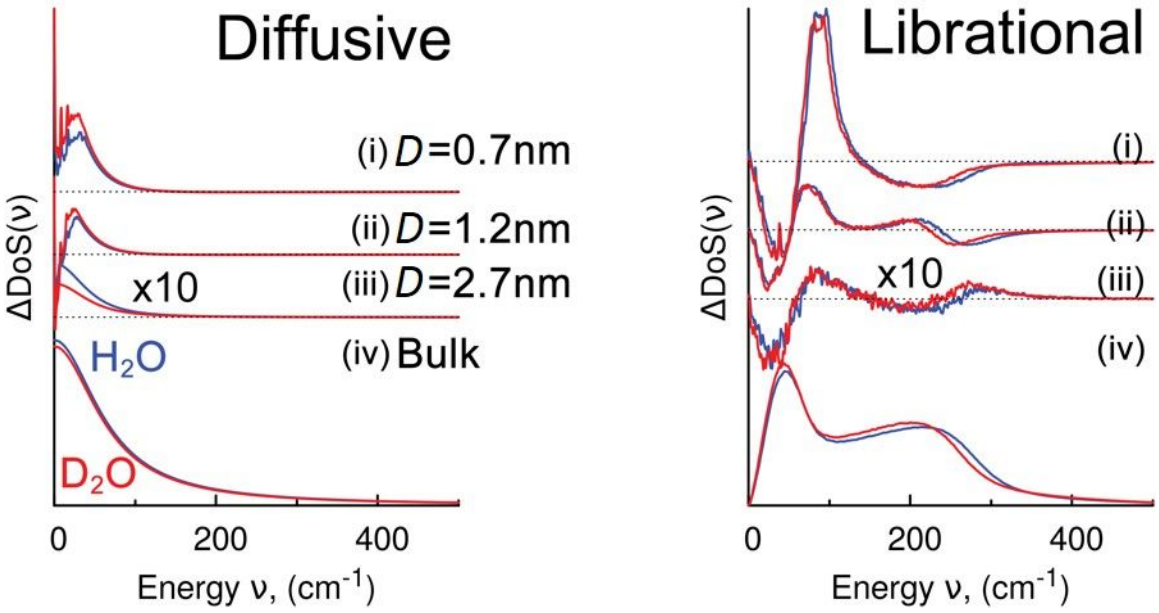

Figure S8: **Density of states function**. **Left panel:** The plot of the per-molecule, excess density of states functions DoS^{ex} for the diffusive modes in nanoconfined H_2O (blue) and D_2O (red). The DoS^{ex} for **(i)** D = 0.7 nm, **(ii)** D = 1.2 nm and **(iii)** D = 2.7 nm (scaled by a factor of 10 to aid visibility), as well as the bulk liquid reference. **Right panel**: The plot of the per-molecule excess density of states functions DoS^{ex} for the librational modes in nanoconfined H_2O (blue) and D_2O (red). Librational motions involve solid-like translations (rattling) motions.

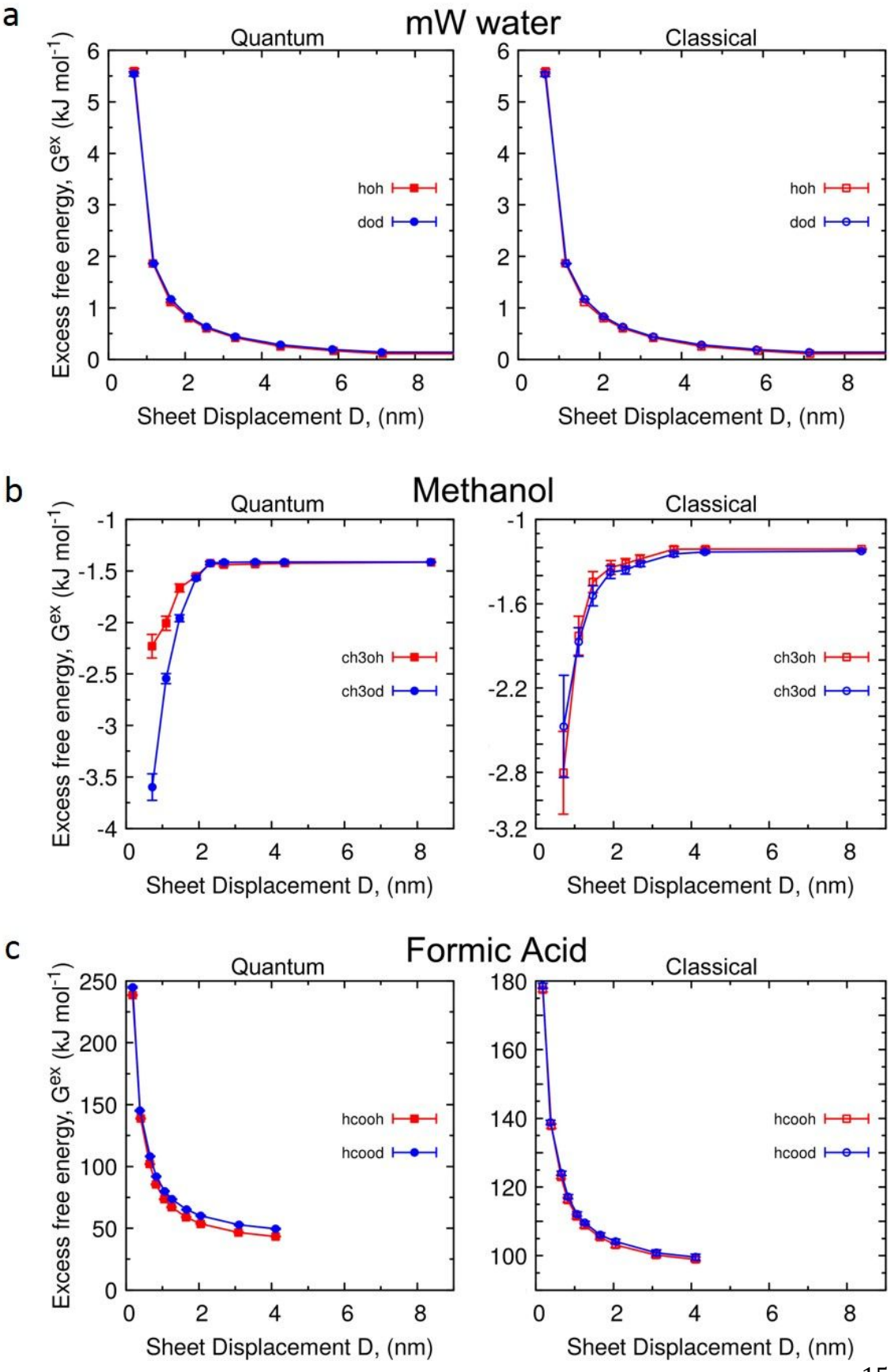
a
mW water
Quantum
Classical
Excess free energy, G^{ex} (kJ mol^{-1})
Sheet Displacement D, (nm)
hoh
dod
b
Methanol
ch3oh
ch3od
c
Formic Acid
hcooh
hcood

Figure S9: NQEs in nanoconfined organic liquids. **(a)**: Excess free energy of D_2O (blue circles) and H_2O (red squares) calculated from MD simulations employing the mW forcefield[23]. The quantum (left) and classical (right) free energies are plotted. The error bars represent standard deviation - 1σ **(b):** Excess free energy of pure liquid methanol described using the OPLS AA/L forcefield[24,25] **(c)** Excess free energy of pure liquid formic acid described using the OPLS AA/L forcefield.

References:

1 Liberelle, B., Banquy, X. & Giasson, S. Stability of Silanols and Grafted Alkylsilane Monolayers on Plasma-Activated Mica Surfaces. *Langmuir* **24**, 3280-3288, doi:10.1021/la703522u (2008).

2 London, G., Carroll, G. T. & Feringa, B. L. Silanization of quartz, silicon and mica surfaces with light-driven molecular motors: construction of surface-bound photo-active nanolayers. *Organic & Biomolecular Chemistry* **11**, 3477-3483, doi:10.1039/C3OB40276B (2013).

3 Wood, J. & Sharma, R. Preparation of a Robust Hydrophobic Monolayer on Mica. *Langmuir* **10**, 2307-2310, doi:10.1021/la00019a047 (1994).

4 Stock, P., Utzig, T. & Valtiner, M. Direct and quantitative AFM measurements of the concentration and temperature dependence of the hydrophobic force law at nanoscopic contacts. *Journal of Colloid and Interface Science* **446**, 244-251, doi:10.1016/j.jcis.01.032 (2015).

5 Soper, A. K. & Benmore, C. J. Quantum differences between heavy and light water. *Physical Review Letters* **101**, 065502, doi:ARTN 065502 10.1103/PhysRevLett.101.065502 (2008).

6 Ceriotti, M. *et al.* Nuclear Quantum Effects in Water and Aqueous Systems: Experiment, Theory, and Current Challenges. *Chemical Reviews* **116**, 7529-7550, doi:10.1021/acs.chemrev.5b00674 (2016).

7 Israelachvili, J. N. *Intermolecular and Surface Forces*. 3rd edn, (2011).

8 Hockney, R. W. & Eastwood, J. W. *Computer simulation using particles*. 1st edn, (Taylor & Francis Group, 1988).

9 Shinoda, W., Shiga, M. & Mikami, M. Rapid estimation of elastic constants by molecular dynamics simulation under constant stress. *Physical Review B* **69**, 134103 (2004).

10 Martyna, G. J., Tobias, D. J. & Klein, M. L. Constant pressure molecular dynamics algorithms. *The Journal of Chemical Physics* **101**, 4177-4189 (1994).

11 Parrinello, M. & Rahman, A. Polymorphic transitions in single crystals: A new molecular dynamics method. *Journal of Applied physics* **52**, 7182-7190 (1981).

12 Tuckerman, M. E., Alejandre, J., López-Rendón, R., Jochim, A. L. & Martyna, G. J. A Liouville-operator derived measure-preserving integrator for molecular dynamics simulations in the isothermal–isobaric ensemble. *Journal of Physics A: Mathematical and General* **39**, 5629 (2006).

13 Berens, P. H., Mackay, D. H., White, G. M. & Wilson, K. R. Thermodynamics and quantum corrections from molecular dynamics for liquid water. *The Journal of Chemical Physics* **79**, 2375-2389 (1983).

14 Pascal, T. A., Lin, S.-T. & Goddard III, W. A. Thermodynamics of liquids: standard molar entropies and heat capacities of common solvents from 2PT molecular dynamics. *Physical chemistry chemical physics* **13**, 169-181 (2011).

15 Vega, C. *et al.* Heat capacity of water: A signature of nuclear quantum effects. *The Journal of Chemical Physics* **132**, 046101 (2010).

16 Ceriotti, M. & Markland, T. E. Efficient methods and practical guidelines for simulating isotope effects. *The Journal of Chemical Physics* **138**, 014112, doi:10.1063/1.4772676 (2013).
17 Shiga, M. & Shinoda, W. Calculation of heat capacities of light and heavy water by path-integral molecular dynamics. *The Journal of Chemical Physics* **123**, 134502 (2005).
18 Cox, J., Wagman, D. & Medvedev, V. Codata Key Values for Thermodynamics, Hemisphere publishing corp., New York, 1, 1984.
19 Salomon, M. Thermodynamic properties of liquid H2O and D2O and their mixtures. Electronics research centre Cambridge, mass. *National aeronautics and space administration, NASA TN D-5223, Washington, DC* (1969).
20 Nemethy, G. & Scheraga, H. A. Structure of water and hydrophobic bonding in proteins. IV. The thermodynamic properties of liquid deuterium oxide. *The Journal of Chemical Physics* **41**, 680-689 (1964).
21 González, M. A. & Abascal, J. L. A flexible model for water based on TIP4P/2005. *The Journal of Chemical Physics* **135**, 224516 (2011).
22 Mayo, S. L., Olafson, B. D. & Goddard, W. A. DREIDING: a generic force field for molecular simulations. *Journal of Physical chemistry* **94**, 8897-8909 (1990).
23 Molinero, V. & Moore, E. B. Water modeled as an intermediate element between carbon and silicon. *The Journal of Physical Chemistry B* **113**, 4008-4016 (2008).
24 Jorgensen, W. L. & Tirado-Rives, J. The OPLS [optimized potentials for liquid simulations] potential functions for proteins, energy minimizations for crystals of cyclic peptides and crambin. *Journal of the American Chemical Society* **110**, 1657-1666 (1988).
25 Kaminski, G. A., Friesner, R. A., Tirado-Rives, J. & Jorgensen, W. L. Evaluation and reparametrization of the OPLS-AA force field for proteins via comparison with accurate quantum chemical calculations on peptides. *The Journal of Physical Chemistry B* **105**, 6474-6487 (2001).